

CHALMERS



Tracking the maximum power point of solar panels

A digital implementation using only voltage measurements

Master of Science Thesis

ERIK LIEDHOLM

Department of Signals and Systems
Division of Automatic Control
CHALMERS UNIVERSITY OF TECHNOLOGY
Göteborg, Sweden, 2010
Report No. EX010/2010

Tracking the maximum power point of solar panels
A digital implementation using only voltage measurements
ERIK LIEDHOLM

©ERIK LIEDHOLM, 2010

Master Thesis at Chalmers University of Technology

Technical report no EX010/2010
Department of Signals and Systems
Chalmers University of Technology
SE-412 96 Göteborg
Sweden
Telephone + 46 (0)31-772 1000

Cover picture:
Measurement platform at a parkinglot on a sunny day in Göteborg

Chalmers Reproservice
Göteborg, Sweden 2010

Abstract

This thesis deals with the problem of attaining high power output from solar panels by employing a maximum power point tracker. The purpose being to propose a viable technique that tracks the maximum power point using only voltage measurements as well as investigating the possibility to control several solar panels individually employing only one actuator. Using a custom measurement circuit and a data acquisition device connected to a LabVIEW program, the characteristics of eight solar panels were monitored for a month. The measurement data was then used in Matlab simulations to evaluate a specific maximum power point tracker called incremental conductance. Some other tracking algorithms were also studied, but only the most promising one was implemented. The incremental conductance algorithm was successfully implemented using only voltage measurements and 94.74% of the electrical power from the solar panels throughout January 2010 was harvested in the most prosperous simulation. Further, using only one actuator to control four solar panels at their individual maximum power points was shown to be possible.

Preface

The thesis work has been carried out at Amparo Solutions AB and their parent company Qamcom Technology AB, with the intent to improve solar power efficiency on their existing traffic safety products.

I would like to thank my supervisors at the companies, Ph.D. Roger Malmberg (Qamcom) and Samuel Munkstedt (Amparo), for their dedication to this project. I am also grateful for the at least as dedicated guidance given by Fredrik Malmsten (Qamcom). Appreciation also goes out to Prof. Bo Egardt for valuable discussions concerning control theory. A special thank you to my parents for supporting me, not only during this thesis, but throughout all of the studies that have brought me this far. I would furthermore like to thank my parents for letting me mount the measurement equipment on the roof of the house.

Erik Liedholm

Göteborg, Sweden, March 2010

Contents

1	Introduction	1
1.1	Background	1
1.2	Purpose	1
1.3	Method	1
1.4	Limitations	1
2	Theory	3
2.1	Photovoltaic cells	3
2.1.1	Equivalent circuits	3
2.1.2	Parameter extraction	5
2.1.3	Partial shadowing	5
2.2	Maximum power point tracker	6
2.2.1	Perturb and observe	6
2.2.2	Ripple correlation control	6
2.2.3	Incremental conductance	6
2.3	Power converters	7
2.4	Implementation hardware	8
3	Method	9
3.1	Measurement platform	9
3.1.1	Requirement specification	9
3.1.2	Design specification	9
3.2	Modeling the solar panels	11
3.3	MPPT	11
3.3.1	Measurements	11
3.3.2	Selection of MPPT	11
3.3.3	Multiple panels with one DC-DC	12
3.4	Simulation	14
3.4.1	Input data	14
3.4.2	Stability in cases of high solar insolation	14
3.4.3	Multiple panels with one DC-DC	14
3.4.4	Simplifications	14
4	Results	17
4.1	Measurements	17
4.1.1	MPP	17
4.1.2	Deviation from MPP	17
4.2	Simulations	19
4.2.1	Step size	19
4.2.2	MPPT	19
4.2.3	Stability in case of high solar insolation	20
4.2.4	Multiple panels with one DC-DC	20
5	Conclusions	23
5.1	Future work	23
A	Solar panels	27
B	Measurement circuit	28

Abbreviations

DAQ	Data acquisition
DC	Direct current
DC-DC	Direct current to direct current
MPP	Maximum power point
MPPT	Maximum power point tracker
P&O	Perturb and observe
RCC	Ripple correlation control

1 Introduction

1.1 Background

The foundation for solar cells was laid in 1839, when the photovoltaic effect was discovered by E. Becquerel. In 1958, over a century later, Vanguard I was launched as the first satellite powered by solar cells [14]. A great deal of research has since then been carried out within the field of photovoltaics, where some of this research has addressed maximization of the power outtake [3].

When harvesting solar energy by the means of electrical solar cells, several parameters must be optimized to attain high power output. One of the main issues is that the power obtained from a solar cell varies with the electrical load applied to the cell, and it is therefore important to operate at a load that gives maximal power. This operating point is affected by numerous conditions, for example temperature, light intensity and light incidence angle. [11]

1.2 Purpose

The aim of this thesis is to propose a viable technique to track the maximum power operating point. This technique should be implementable on a specific hardware platform that lacks current sensors. The possibility to control several panels individually with only one actuator should also be investigated

1.3 Method

The characteristics of the solar panels are measured using several sensors and a custom circuit for automatic switching between panels. Available methods for tracking the maximum power point are reviewed and evaluation of the proposed method is done by simulations against measurement data in Matlab.

1.4 Limitations

The evaluation of the proposed method has been carried out by computer simulations, since implementation on the real hardware is outside the scope of this thesis. The real world measurements have been limited to one type of solar panels, since the solar panel selection has already been done by Amparo Solutions AB.

2 Theory

2.1 Photovoltaic cells

Photovoltaic (PV) cells, commonly called solar cells, are made up of semiconducting materials and generate electrical energy when illuminated by light. The amount of power being generated depends on several external parameters, where the intensity of the illumination is the most important, but temperature and incidence angle does also have impact. Moreover the power output from the cell is voltage dependent as illustrated in Fig. 2.1, which implies that the choice of operation voltage is very important.

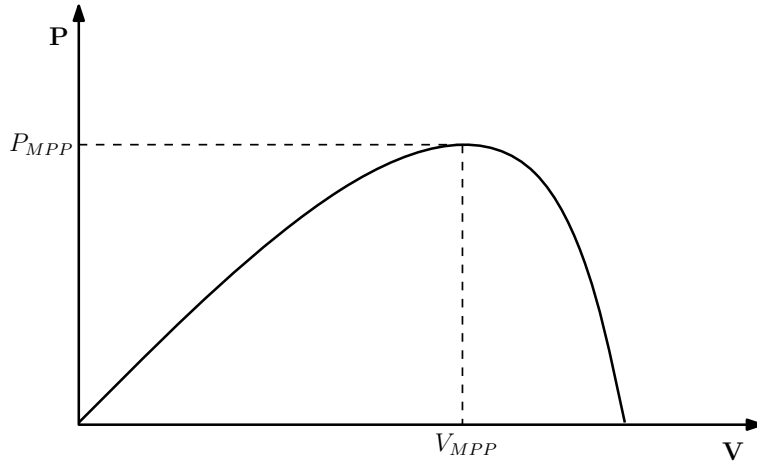


Figure 2.1: Typical Power-Voltage curve for a photovoltaic cell

At the Maximum Power Point (MPP) the voltage is known as V_{MPP} and this voltage is also influenced by the external parameters affecting the cell. The problem of a varying V_{MPP} is usually solved by employing a Maximum Power Point Tracker (MPPT), presented in section 2.2.

The power generation is instantaneous when illuminated and the cell itself cannot store any energy. To clarify the terminology, combining multiple solar cells results in a solar panel, and several solar panels forms a solar panel array [11].

2.1.1 Equivalent circuits

Numerous equivalent circuits are available that try to characterize the behavior of photovoltaic cells, shown in Fig. 2.2. Most of the equivalent circuits are variations of the basic model called the single diode model [15]. One version of the single diode model is shown in Fig. 2.3 and can be described by (2.1), where I_{ph} is the current generated by the incoming light, I_0 is the diode reverse saturation current, n is the diode ideality factor, V_{th} is the thermal voltage, R_s is the series resistance and G_s is the shunt conductance [13]. The thermal voltage is defined as $V_{th} = \frac{kT}{q}$ where k is the Boltzmann constant ($1.3806504 \cdot 10^{-23} \frac{J}{K}$), T is the temperature in degrees Kelvin and q is the elementary charge ($1.602176487 \cdot 10^{-19} C$) [12].

$$I = I_0 \left[\exp \left(\frac{V - IR_s}{nV_{th}} \right) - 1 \right] + (V - IR_s)G_p - I_{ph} \quad (2.1)$$

This specific version of the single diode model was chosen to match the parameter extraction procedure described in section 2.1.2.

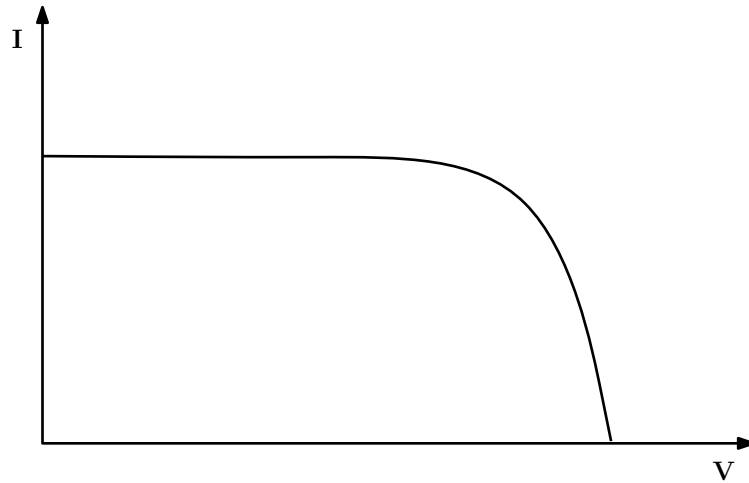


Figure 2.2: Typical Current-Voltage curve for a photovoltaic cell

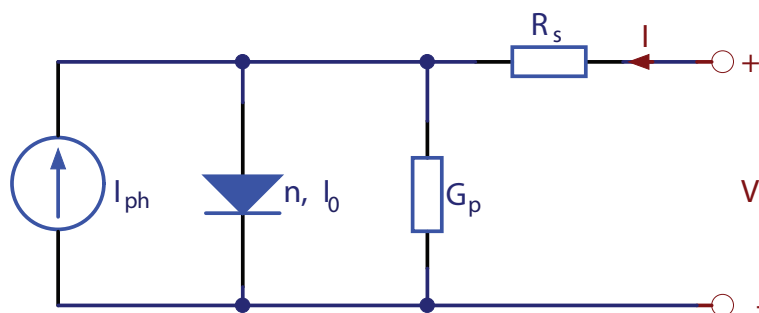


Figure 2.3: Single diode equivalent circuit for a photovoltaic cell [13]

2.1.2 Parameter extraction

The parameters shown in the equation for the equivalent circuit (2.1) are not always given by the manufacturer of the solar panels. When such data is absent parameter extraction from measurements can be used to calculate these values. The equivalent circuit model (2.1) expresses the current in terms of the voltage, and the current is present at both sides of the equality sign. This poses a problem, since this formula can not be rewritten as explicit functions of current and voltage without using so called Lambert W functions, which are unsuitable for parameter extraction by numerical fitting [13]. There is an already developed parameter extraction method, presented by [13], that does not use Lambert W functions.

While the implementation of the method will be presented below, the theory behind the formulas are left for the interested reader to study from the original paper.

This method concerns creating a function from measurement data, called the co-content function (2.2), where I_{sc} is the short-circuit current and the lower limit of the integral is defined at $V = 0$ and $I = I_{sc}$.

$$CC(V) = \int_0^V (I(\epsilon) - I_{sc})d\epsilon \quad (2.2)$$

By using a current-voltage characteristic measurement, defined by two vectors \mathbf{I} and \mathbf{V} , the co-content function is created by evaluating the integral of (2.2) for every set (I, V) of the vectors. To further clarify, each measurement set consists of values I and V , acquired at the same time; for a specific V there is a matching I .

After the co-content function has been calculated, it is numerically fitted to (2.3), where $C_{I1V1} = \frac{1 - \sqrt{1 + 16C_{V2}C_{I2}}}{2}$.

$$CC(V) = C_{V1}V + C_{I1}(I(V) - I_{sc}) + C_{I1V1}V(I(V) - I_{sc}) + C_{V2}V^2 + C_{I2}(I(V) - I_{sc})^2 \quad (2.3)$$

The fitting will produce values for the co-content coefficients $C_{V1}, C_{V2}, C_{I1}, C_{I2}$ and the sought data can then be extracted using the following formulas:

$$G_p = 2C_{V2} \quad (2.4)$$

$$R_S = \frac{\sqrt{1 + 16C_{V2}C_{I2}} - 1}{4C_{V2}} \quad (2.5)$$

$$n = \frac{C_{V1}(\sqrt{1 + 16C_{V2}C_{I2}} - 1) + 4C_{I1}C_{V2}}{4V_{th}C_{V2}} \quad (2.6)$$

$$I_{ph} = -\frac{(1 + \sqrt{1 + 16C_{V2}C_{I2}})(C_{V1} + I_{sc})}{2} - 2C_{I1}C_{V2} \quad (2.7)$$

I_0 is then calculated in (2.8) using the extracted parameters, where V_{oc} is the open circuit voltage.

$$I_0 = \frac{I_{ph} - V_{oc}G_p}{\exp\left(\frac{V_{oc}}{nV_{th}}\right)} \quad (2.8)$$

2.1.3 Partial shadowing

When several solar cells are connected in series, shading some of the cells will result in significant power reduction [16]. As seen in section 2.1.1, photovoltaic cells function as current sources coupled in parallel with a diode. When a cell is shaded and therefore produce less current than the other cells, the excess current will force the diode into reverse bias and finally into breakdown operation. A diode normally lets current flow in one direction only, but when the diode is in breakdown the current is allowed to flow in the opposite direction. Reversed bias operation will heat the diode and possibly damage the solar cell [6]. Furthermore partially shaded solar panels can exhibit several maximas in its power-voltage characteristic which complicates the process of tracking the MPP [3].

2.2 Maximum power point tracker

There exist several techniques for tracking the MPP of a photovoltaic array. These techniques are commonly referred to as MPPTs, maximum power point trackers [3]. Some MPPT approaches (considered feasible for this thesis) are explained below.

2.2.1 Perturb and observe

Perturb and observe (P&O) is a widely used technique because of it being intuitive and easy to implement. The fundamental P&O method concerns measuring voltage and current from the solar panel while perturbing the operating voltage and comparing the power received at the new voltage with the power received at the old voltage. If higher power was measured at the new voltage the next perturbation will be in the same direction as the last, it will otherwise go in the opposite direction. This technique employs a fixed step size, and choosing this size will lead to a tradeoff between convergence speed and oscillation size. If using large steps in the perturbations, the convergence to the MPP will be fast, but the system will oscillate around the MPP; smaller steps will result in slower convergence and smaller oscillations.

If using a power converter, changing of the operating voltage is done indirectly by changing the duty cycle of the power converter which will affect the amount of current drawn from the panel; when the P&O method is applied to such a setup it is called hill-climbing [3].

2.2.2 Ripple correlation control

Ripple Correlation Control (RCC) is a variation of a control approach called Extremum seeking. When using a switching power converter, ripple from the switching will be induced in the system, and information of this ripple can be used to adjust the duty cycle of the power converter.

One implementation of RCC uses the time derivatives of the received power and current to set the duty-cycle of the power converter (2.9)

$$d(t) = k \int \frac{dP}{dt} \frac{dI}{dt} dt \quad (2.9)$$

In order for the RCC algorithm to work, the ripple must be captured by sampling data close to the points where the switching occurs [2].

2.2.3 Incremental conductance

Incremental conductance uses the fact that the power derivative with respect to voltage will be equal to zero at the MPP and positive for voltages below the MPP as well as negative for voltages above the MPP (2.10), something that is easily realized if looking at the power-voltage curve presented in Fig. 2.1.

$$\begin{cases} \frac{dP}{dV} = 0 & \text{at MPP} \\ \frac{dP}{dV} > 0 & \text{left of MPP} \\ \frac{dP}{dV} < 0 & \text{right of MPP} \end{cases} \quad (2.10)$$

Since $P = IV$, the power derivative with respect to voltage can be expressed as (2.11) and (2.10) can therefore be realized as (2.12), which states that the incremental conductance is equal to the negative of the instantaneous conductance at the MPP.

$$\frac{dP}{dV} = \frac{d(IV)}{dV} = I \frac{dV}{dV} + V \frac{dI}{dV} = I + V \frac{dI}{dV} \cong I + V \frac{\Delta I}{\Delta V} \quad (2.11)$$

$$\begin{cases} \frac{\Delta I}{\Delta V} = -\frac{I}{V} & \text{at MPP} \\ \frac{\Delta I}{\Delta V} > -\frac{I}{V} & \text{left of MPP} \\ \frac{\Delta I}{\Delta V} < -\frac{I}{V} & \text{right of MPP} \end{cases} \quad (2.12)$$

Using (2.12), the incremental conductance algorithm is defined as shown in Fig. 2.4.

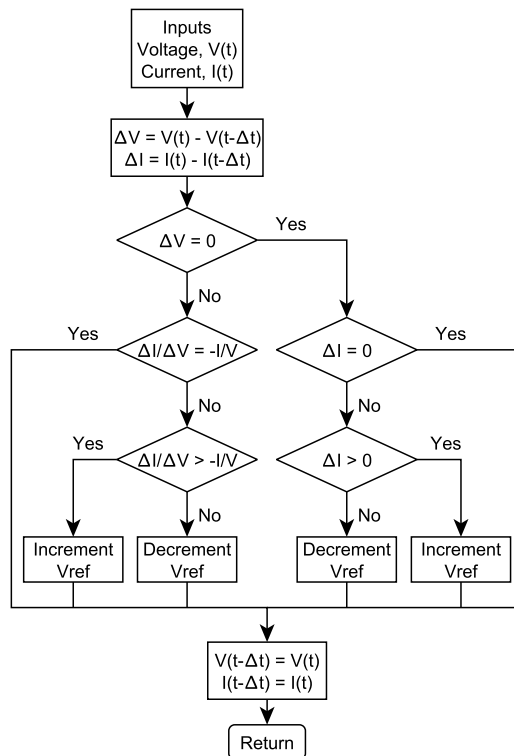


Figure 2.4: Incremental conductance algorithm as shown in [3, 7, 9]

Just as P&O, incremental conductance uses fixed step lengths when changing the operating voltage so this algorithm also has the tradeoff between convergence time and oscillation size. However unlike P&O, incremental conductance checks for change in voltage (ΔV) and thereby senses if the MPP has moved. [3, 7, 9].

2.3 Power converters

The aim of power converters is to convert electric power from one form to another with high efficiency. The system considered in this thesis harvests energy from solar panel and stores it in batteries. Since the voltage from the solar panels can be much higher than the battery voltage, a suitable power converter must be used. Both the solar panels and batteries operate on DC, therefore a power converter that converts DC-voltage to lower DC-voltage would be suitable; such a converter is called direct current to direct current (DC-DC) buck converter. A buck converter is one of the simplest types of power converters. The input voltage is switched on and off at a fixed frequency to get a lower output voltage. To avoid ripple from the switching propagating on the output voltage, a low pass filter is used. The power converter itself can be switched on or off and this is how the level of the output voltage is controlled, usually implemented by setting a duty-cycle that controls how often the power converter is switched on.[1].

2.4 Implementation hardware

There is a predefined hardware platform that the MPPT will run on. In Fig. 2.5 the basic interface to the solar panel is shown, where the panel is connected in parallel with a capacitor and a DC-DC converter. The voltage over the capacitor can be measured but there is no current sensor, instead the current can be estimated by observing the voltage difference of the capacitor with respect to time. The DC-DC can be set to four discrete current levels which control the average current drawn from the capacitor and the DC-DC can in addition be switched on or off. Estimation of the current is further explained in section 3.3.1.

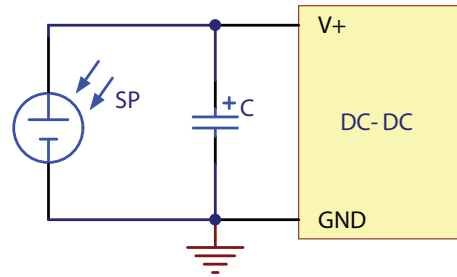


Figure 2.5: Outline of the implementation hardware platform

3 Method

3.1 Measurement platform

When measuring the characteristics of the solar panels a data acquisition (DAQ) device was used to get measurements into the computer and change the load on the panels via a custom circuit. Sensors for temperature and illumination were also used.

The DAQ and the circuit were fitted inside of an aluminum box with 8 solar panels mounted according to Fig. 3.1.

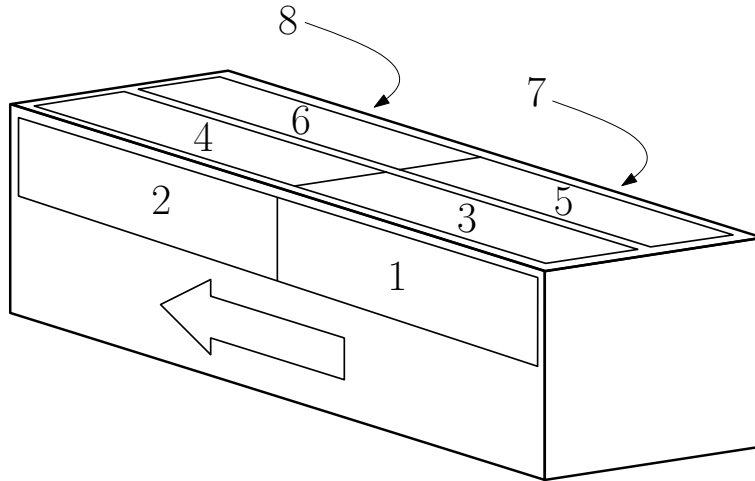


Figure 3.1: Placement of the eight panels on the measurement platform

3.1.1 Requirement specification

The requirement specification is presented in table 3.1 and was created from previous measurements done by Amparo Solutions. Voltage, current, temperature and illumination are parameters to be measured and load is a parameter that will be controlled.

	Range	Resolution	Accuracy
Voltage	5 - 30V	0.01V	$\pm 0.1V$
Current	1 - 80mA	0.01mA	$\pm 0.1mA$
Load	1 - 80mA	0.01mA	$\pm 0.1mA$
Temperature	0 - 50°C	1°C	$\pm 2.5^\circ C$
Illumination	0 - 150mW/cm ²	0.01mW/cm ²	$\pm 0.1mW/cm^2$

Table 3.1: Requirement specification

At an illumination of 100mW/cm², each of the solar panels will generate an open-circuit voltage of 24.5V, a short-circuit current of 60mA and nominal power of 820.5mW. These values cannot be considered the maximum output of the arrays, since the illumination can go above 120mW/cm² [4].

3.1.2 Design specification

To be able to switch between the panels and to vary the load, a custom circuit was designed. The circuit is controlled by a DAQ device, NI USB-6212, which sets the load, what panel to be connected and samples measurements. The DAQ device is in turn controlled by a computer running

a measurement program developed in a programming language called LabVIEW from National Instruments. The circuit loops through the connected panels one by one, connecting them to the load and logging temperature, illumination, current and voltage. To reduce measurement errors caused by transient behavior, the system waits some time after changing load and switching panel before measuring. A description of the measurement process is presented as a flowchart in Fig. 3.2

The requirement specification was used as a guide when designing the custom circuit of which full schematics and component list can be found in appendix B.

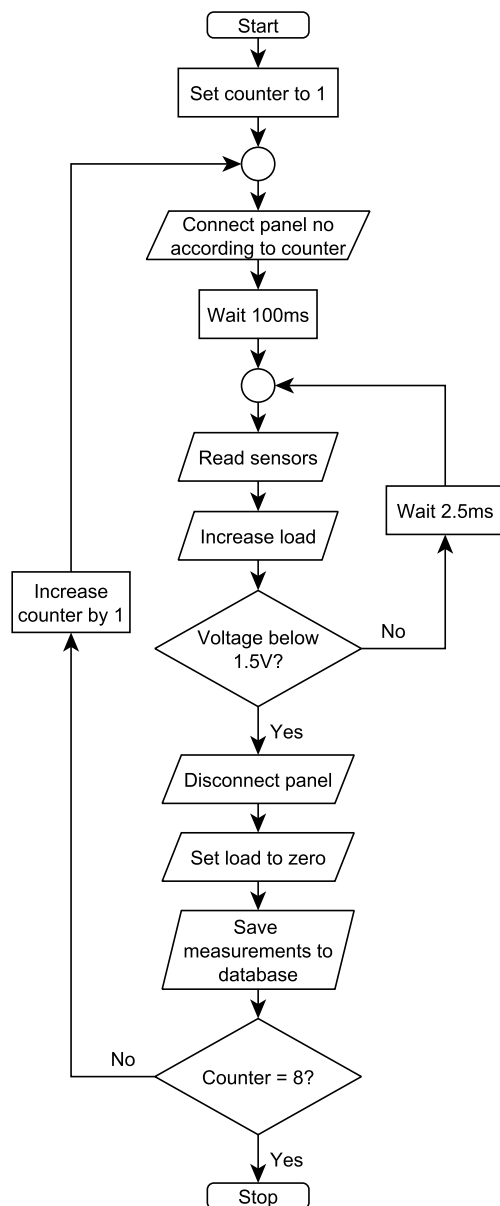


Figure 3.2: Measurement program

3.2 Modeling the solar panels

The solar panels were modeled according to the equivalent circuit from section 2.1.1. Since no data about the sought parameters were given by the manufacturer, parameter extraction had to be used in order to approximate these quantities. The parameter extraction was carried out in Matlab using the method described in section 2.1.2.

3.3 MPPT

3.3.1 Measurements

On the intended hardware platform the voltage is directly measurable, but the current is not. Since knowledge about the current is needed in order to implement any of the MPPTs shown in section 2.2, the current must be estimated.

Consider Fig. 3.3 that illustrates the voltage of the capacitor over time. When the capacitor voltage goes above a specified level V_{ref} , the DC-DC is switched on and the capacitor is discharged for t_{dch} s. The DC-DC is then switched off and the capacitor is charged for t_{ch} s. The resulting increase in voltage ΔV_{ch} can then be multiplied by the capacitance value C and divided by the time t_{ch} to get the average current \bar{I}_c fed into the capacitor during the charging (3.1). Considering that \bar{I}_c is not an instantaneous value, but an average value over t_{ch} , it makes sense to use an average value of V during this time as well. Voltage measurements are made before switching on the DC-DC (V_b) and right after it has been switched off (V_a). The average voltage level during the charging can thus be expressed by the half of the voltage change plus the voltage level at the beginning of the charging (3.2).

$$\bar{I}_c = C \frac{\Delta V_{ch}}{t_{ch}} = C \frac{V_b - V_a}{t_{ch}} \quad (3.1)$$

$$\bar{V}_c = \frac{\Delta V_{ch}}{2} + V_a = \frac{V_a + V_b}{2} \quad (3.2)$$

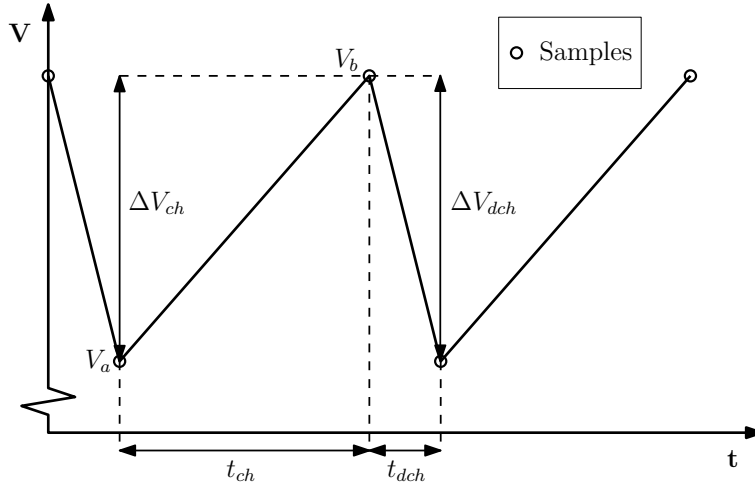


Figure 3.3: Two charge cycles of a capacitor

3.3.2 Selection of MPPT

From the results presented by [10], RCC is superior to methods using fixed step sizes such as Incremental Conductance and P&O. Unfortunately RCC cannot be easily implemented on this setup since the algorithm relies on the ripple induced by the switching of the power converter to

function. The problem lies in the current estimation presented in section 3.3.1, which will eliminate the ripple. Fig. 3.4 shows possible data points to be collected using a current sensor and using the estimation. It would be possible to capture some of the ripple characteristics by performing the estimations more frequently than once on each slope. This would require at least the double sampling rate of other methods, hence being able to use RCC will raise power consumption of the control circuitry and the advantage of this method on this specific hardware platform is doubtful. Considering the increased sampling rate required for RCC and the lack of sensing MPP movements for P&O, incremental conductance is favored and therefore chosen as the technique that will be implemented.

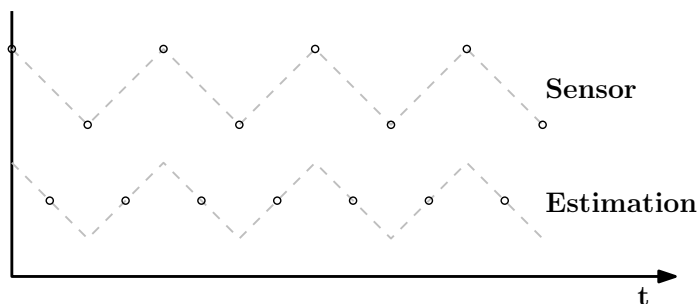


Figure 3.4: Current measurements using sensor or estimation

3.3.3 Multiple panels with one DC-DC

From an academic point of view it was investigated if several panels could use one common DC-DC and still be able to operate each panel at its individual MPP. Based on the same hardware setup shown in section 2.4; The idea is to switch between panels while the capacitors are charging. Each solar panel will have its own capacitor.

Size of timeslots Given a large enough capacitor and large enough current setting on the DC-DC, the charging process will take much longer than the discharge, i.e. $t_{dch} < t_{ch}$, see Fig. 3.3 for a clarification. Fig. 3.5 shows the principle applied using three solar panels; the DC-DC is switched on for a limited time t_{dch} to discharge the capacitor of panel A and the panel is then electronically switched for panel B. The newly connected capacitor is discharged in the same way as the last one but for a possible different t_{dch} suitable for this particular panel. This procedure is then repeated for panel C and then starts over with A.

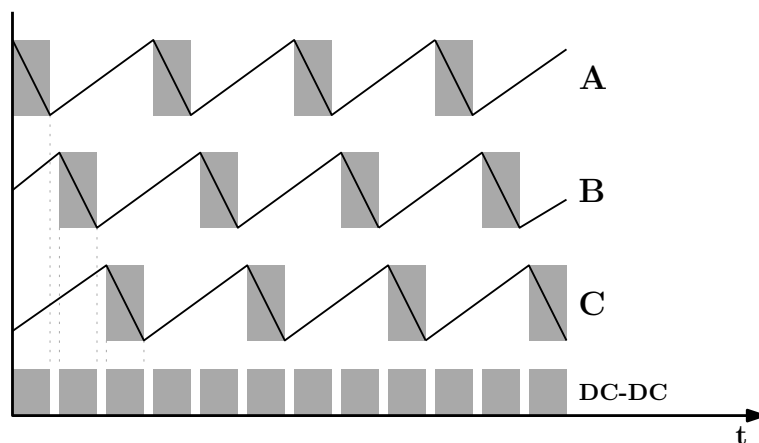


Figure 3.5: Three solar panels time slotted to share one DC-DC

To simplify the system, fixed timeslots of equal sizes are presumed. Within a panel's timeslot the DC-DC can be switched on, but it does not have to be on the whole time, or be switched on at all. The worst possible case is when the DC-DC has to be on the whole time in order to drain the capacitor to the desired level. Considering a capacitor of C farad, fed with $i(t)$ ampere for a period of t seconds will exhibit a change in voltage ΔV according to (3.3) [8].

$$\Delta V = \frac{i(t)}{C}t \quad (3.3)$$

In this case $i(t) = I_{dcdc}(t) - I_p(V_p(t))$, where $I_{dcdc}(t)$ is the current drawn by the DC-DC and $I_p(V_p(t))$ is the current fed by the solar panel. This gives the minimum size of the timeslot (3.4).

$$t > \frac{\Delta V_{dch}}{I_{dcdc}(t) - I_p(V_p(t))}C \quad (3.4)$$

Since the panels are cycled through in a fixed order, the maximum possible rise in voltage of a disconnected panel sets the upper bound of the timeslot size. This upper bound can be expressed by (3.5), where n represents the number of panels.

$$t < \frac{\Delta V_{ch}}{I_p(V_p(t))(n-1)}C \quad (3.5)$$

The limits of the timeslots are considered at steady state operation, hence the size of ΔV_{ch} and ΔV_{dch} are regarded as equal.

Timeslot timing The scenario shown in Fig. 3.5, where each panel is perfectly timed to be discharged within its whole timeslot, is not realistic. Given fixed timeslots of the same size and different power output from the panels this would only be possible if the current drawn by the DC-DC could be set to an arbitrary level. This is not considered possible with the intended hardware, so a different approach must be used.

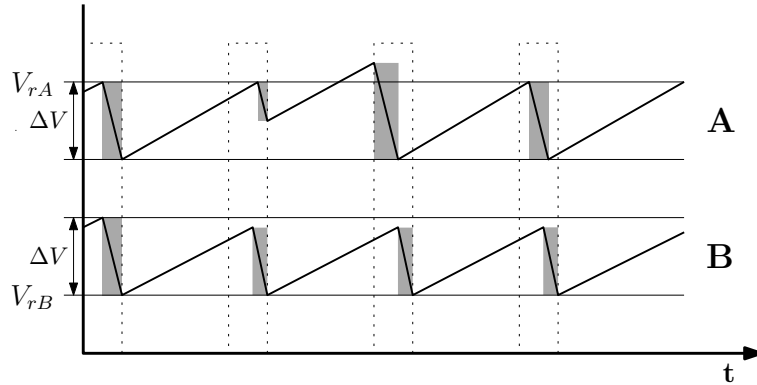


Figure 3.6: Two different ways of triggering DC-DC activation

Fig. 3.6 illustrates two different ways of handling this problem. The areas enclosed by the dotted lines define the timeslots and the gray areas define when the DC-DC is active. Method A uses an upper threshold V_{rA} to define the operating point. As soon as the voltage goes above V_{rA} the DC-DC is switched on until the voltage goes to $V_{rA} - \Delta V$. This will work fine as long as V_{rA} is reached in good time within a timeslot, but when V_{rA} is reached in the end of a timeslot there will not be enough time left to discharge to $V_{rA} - \Delta V$, as can be seen in the second timeslot. This results in an overshoot present in the next timeslot and unpredictable regulation. Method B aims to always have brought the voltage down to V_{rB} at the end of each timeslot. The time it will take to discharge from the current voltage level down to V_{rB} is calculated repeatedly within the timeslot. When this time equals the time that is left of the timeslot, the DC-DC is started.

This regulation will result in a steady voltage shape. Since the panels being controlled can have big differences in power output due to e.g. partial shading, it would be beneficial to skip a panel in the cycle if it is predicted not to rise above a specified level of ΔV within its timeslot.

3.4 Simulation

To validate and tune the control design a simulation environment was developed in Matlab. The charging of the capacitor is simulated by using the relation (3.3), where $i(t)$ is the difference between the current from the solar panels and the current drawn by the DC-DC; the capacitor size is set to $500\mu\text{F}$. In connection to the simulation of physical properties as described above, the incremental conductance MPPT is simulated by employing the algorithm in Fig. 3.7. Though not explicitly shown, the algorithm incorporates the current estimation and average voltage calculation from section 3.3.1. The sampling is simulated with a frequency of 1kHz.

3.4.1 Input data

The panel characteristics are known from measurement series performed every 15 minutes throughout January 2010, using the measurement algorithm shown in Fig. 3.2. The characteristic describes what current the panel generates at a specific voltage; the typical appearance of such measurement series has already been presented in Fig. 2.2. These measurement series are in practice used as three-dimensional lookup tables during the simulation, to evaluate what current the panel generates at a specific time and voltage level. Since a 15 minute resolution of the time variable in the lookup table is quite coarse, a two-dimensional linear interpolation was implemented using the Matlab command *interp2* allowing stepless approximation in between two measurement series.

3.4.2 Stability in cases of high solar insolation

The MPPT algorithm will be tested having measurement data from January 2010 as input. Successfully simulating through the whole of January will ensure that the algorithm works even in low solar insolation, which will be the case in the end and beginning of each day. Since the highest solar insolation is attained in the summer, and January is part of the winter in Sweden, a special simulation is required to test the algorithm for high solar insolation. By employing the parameter extraction method described in section 2.1.2 and altering the I_{ph} value, characteristics from a sunny day can be generated.

3.4.3 Multiple panels with one DC-DC

To simulate several panels being controlled using only one DC-DC, a similar approach to the algorithm shown in Fig. 3.7 was used. The difference being that after turning off the DC-DC and saving voltage measurement with a timestamp, the panel is left to charge its capacitor while switching to another panel. Furthermore the decisions to start and stop the DC-DC is based on Method B that was presented in section 3.3.3 under the topic of *Timeslot timing*.

3.4.4 Simplifications

Since the DC-DC is active for very short periods, its inner characteristics are not modeled and therefore simplified so that it draws the specified current from the exact moment that it is turned on. The calculations carried out by the MPPT algorithm are regarded as atomic and that the atomic operation takes no time. For the case of using several panels, the switching between them is considered to happen instantly and lossless.

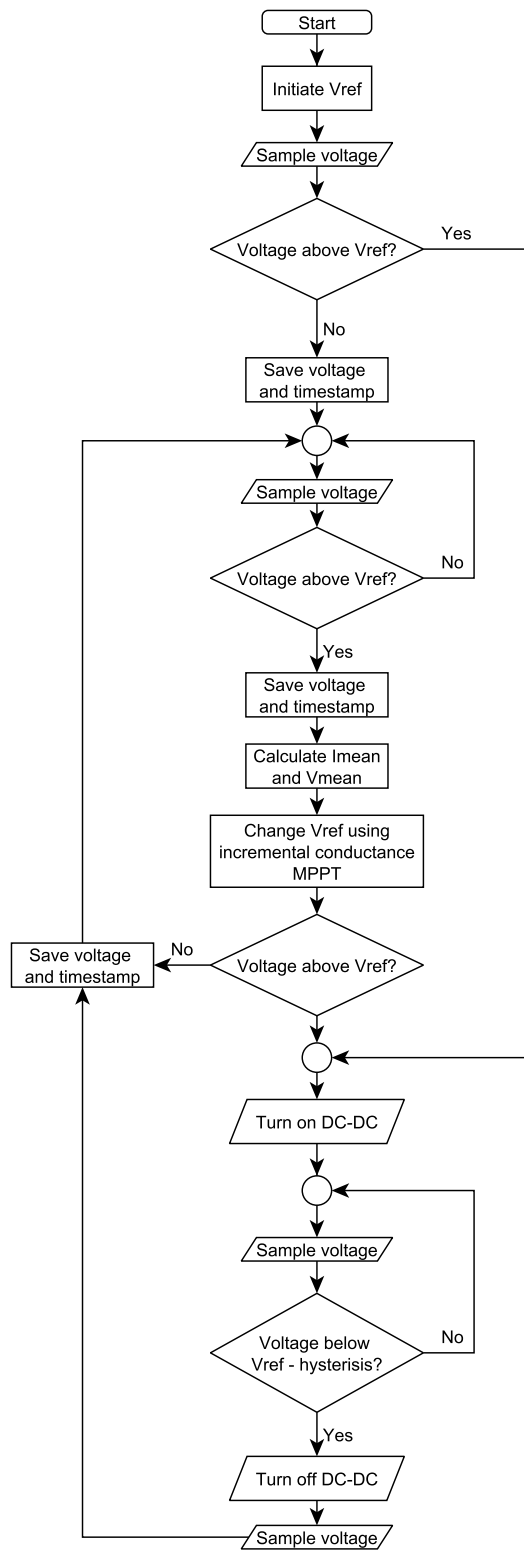


Figure 3.7: MPPT program

4 Results

4.1 Measurements

The measurements used to render the following results were captured once every fifteen minutes throughout January 2010.

4.1.1 MPP

The voltage of the maximum power points for each of the eight panels is presented in the histograms in Fig. 4.1. The distributions are quite narrow except for panels 2 and 8 that are partially shadowed.

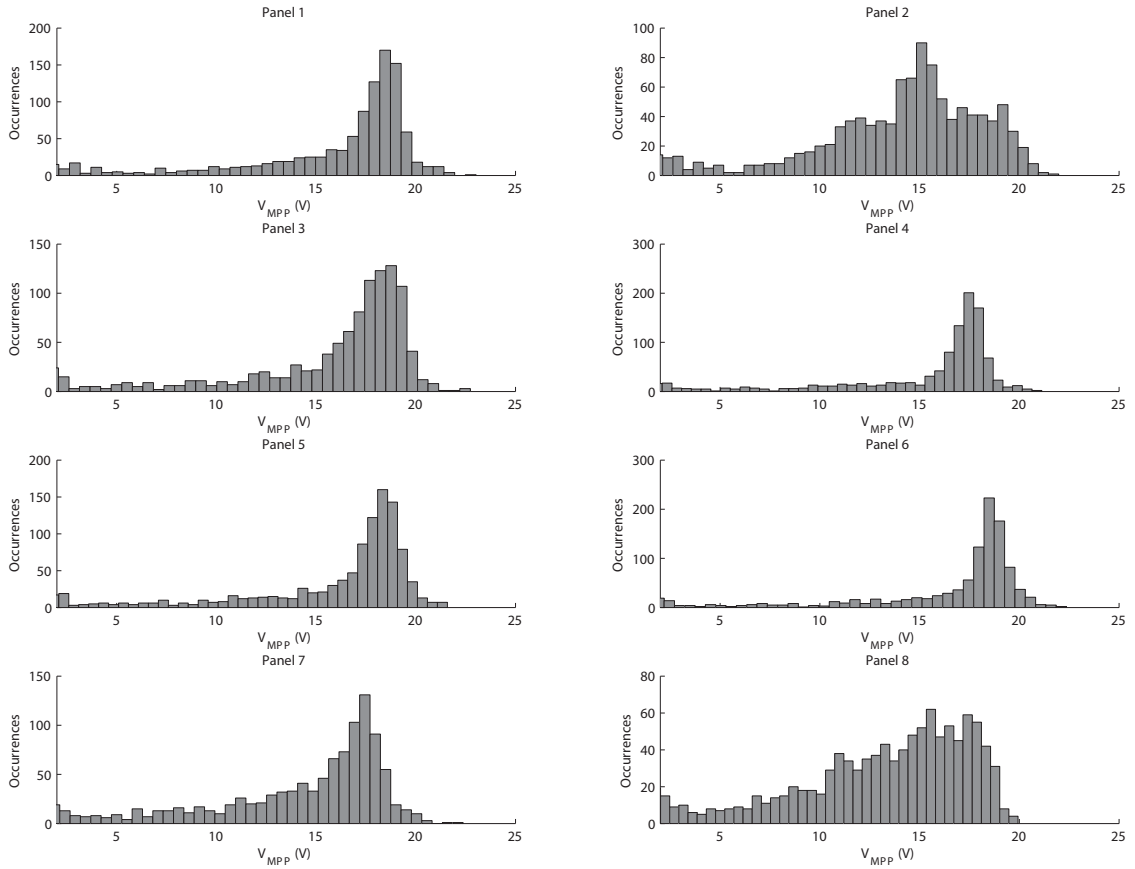


Figure 4.1: V_{MPP} for all panels, where panel 2 and 8 were permanently shadowed by 20%

4.1.2 Deviation from MPP

The momentaneous power outtake can be calculated by (4.1), where a is the deviation from the voltage of the MPP, n is the number of measurement sets and j is the measurement set rendering the power P and MPP voltage, V_{MPP} . Using all of the measurements from January 2010, calculating (4.1) for different a yields the result in Fig. 4.2. It proved to be more forgiving to operate below V_{MPP} than above, when deviating from the MPP.

$$P_{mom}(a) = \frac{1}{n} \sum_{j=1}^n \frac{P_j(V_{jMPP} - a)}{P_j(V_{jMPP})} \quad (4.1)$$

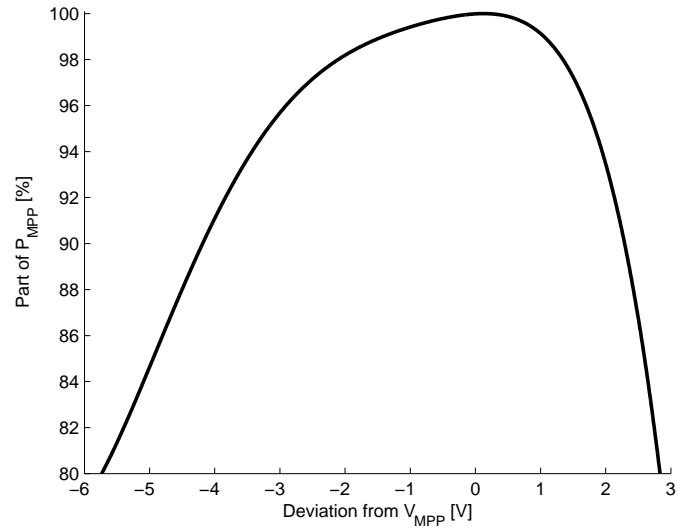


Figure 4.2: Momentaneous power loss by deviation from V_{MPP}

Assuming that V_{MPP} is attained correctly by the MPPT, deciding upon an acceptable ripple size using the average power loss would be a better qualifier than the momentaneous power loss. The average power loss is calculated from the momentaneous power loss by (4.2), where a denotes the symmetric deviation from V_{MPP} and the result is shown in Fig. 4.3.

$$\int_{-a}^a P_{mom}(\epsilon) d\epsilon \quad (4.2)$$

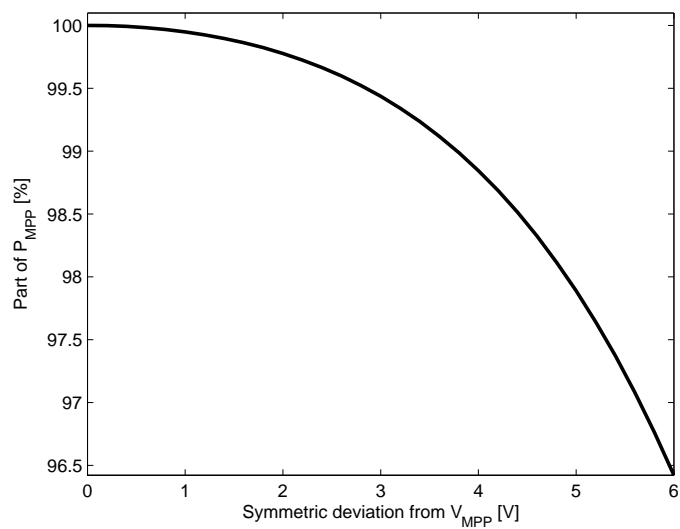


Figure 4.3: Average power loss by symmetric deviation from V_{MPP}

4.2 Simulations

The basis for these simulations is shown in section 3.4.

4.2.1 Step size

To get an idea of how the step size of V_{ref} (V_{rB} in Fig. 3.6) impact speed and ripple, a step responses simulation was carried out. V_{ref} was initiated to 0V and the actual V_{MPP} was 17.3V where P_{MPP} was 0.7W. The resulting power output shown in Fig. 4.4 demonstrates that the rise time is halved when doubling the step size, while the ripple is just slightly increased.

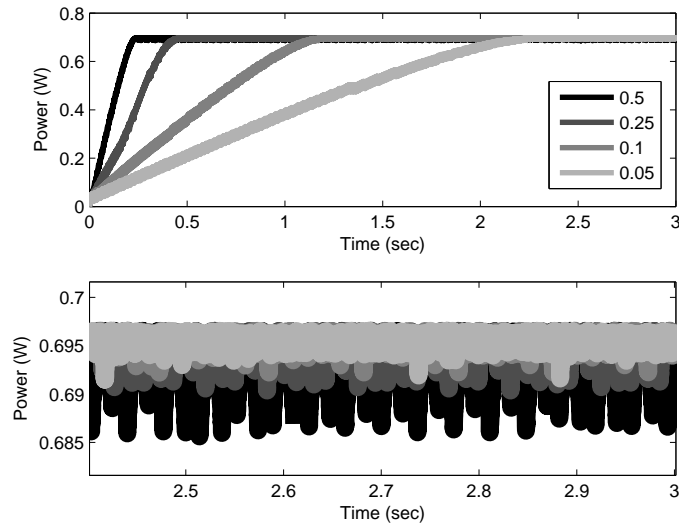


Figure 4.4: Step response from different V_{ref} step sizes

4.2.2 MPPT

The incremental conductance MPPT was simulated with four different step sizes and with the measurement data from panel 5 throughout January 2010 as input. The resulting power outtake is shown in table 4.1, where a 0.5V step size gave the highest power output. As previously mentioned, several maximas can appear when a panel is partially shaded, making it possible for the incremental conductance algorithm to end up in a local maxima; this can be one of the limiting factors for the attained result.

Step size (Volt)	Efficiency (%)
0.75	94.31
0.5	94.74
0.25	92.98
0.1	90.40

Table 4.1: Resulting power outtake using Incremental Conductance MPPT

Calculating the efficiency of the MPPT was done by using the formula (4.3), where P_{MPPT} is the power received when using the MPPT and P_{MPP} is the maximum power available [2].

$$\text{Efficiency} = \frac{\int P_{MPPT}}{\int P_{MPP}} \quad (4.3)$$

4.2.3 Stability in case of high solar insolation

Parameter extraction was performed from a set of data and verified against another set of data. The I_{ph} value, corresponding to the solar insolation, was increased so that the output was twice as high as the panels' maximum rating. A step response was then carried out with the MPPT algorithm configured as previous, but with a higher DC-DC current setting. The simulation result depicted in Fig. 4.5 shows that the algorithm deals with high insolation successfully and quickly finds the MPP.

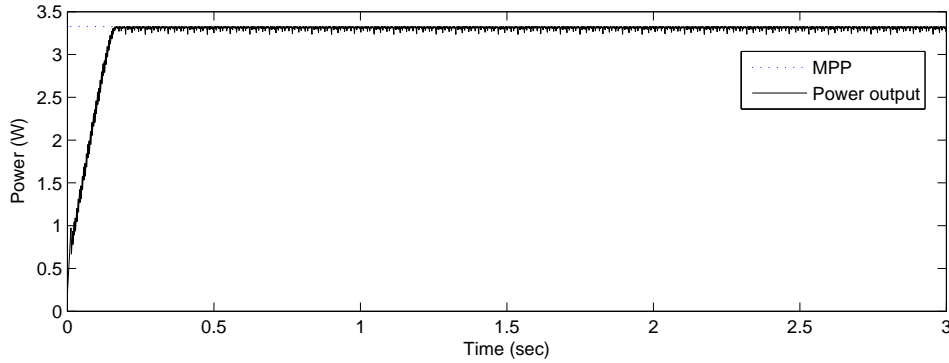


Figure 4.5: Step response in a case of high solar insolation

4.2.4 Multiple panels with one DC-DC

In excess of the approach described in section 3.4.3, the simulation method also features a criterion to select the setting of how much current the DC-DC should draw from the circuit. The criterion was created from trials in the simulation environment. Using the estimated current \bar{I}_c and the fulfillment of (4.4) by two neighboring current settings for the DC-DC, I_a ampere and I_b ampere, the DC-DC should be set to operate at the setting I_b , when using the DC-DC together with n panels. This must in practice be implemented with a hysteresis to avoid frequent switching; Substituting I_b for $I_b - h$ is a possible way to implement this.

$$\frac{I_a}{1.5n} > \bar{I}_c > \frac{I_b}{1.5n} \quad (4.4)$$

The simulation features four panels, which were given characteristics from individual measurement data. Starting off with characteristics from a sunny day, after half of the simulation time the data is swapped for characteristics from a cloudy day. The outcome of the simulation, rendered in Fig. 4.6, display prompt regulation to the individual maximum power points and desired effect of the DC-DC current selection criterion.

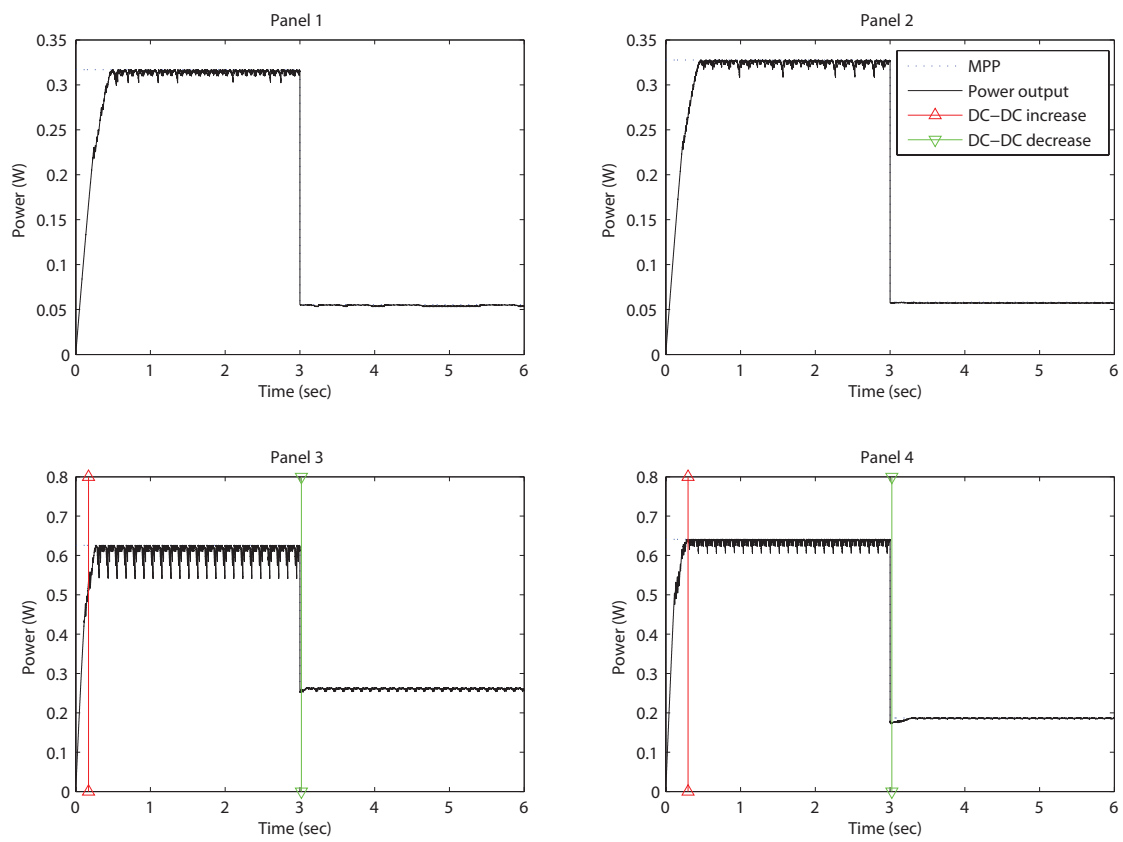


Figure 4.6: Four solar panels being controlled at their individual MPP using only one DC-DC

5 Conclusions

Incremental conductance has by simulations been shown to be a feasible MPPT on a platform lacking current sensors. The method proposed has not been tested against uncertainty of the capacitance value, which might have severe impact of the performance of the MPPT. Although as long as the right choice of direction is taken, there will be no change in performance since a fixed step size is employed, and it is therefore unlikely that the MPPT will be sensitive to small differences of the capacitance in the model versus the actual capacitance. Complementing the incremental inductance algorithm with some way of ensuring that the current maxima is the global one will probably improve the performance when operating at partially shaded conditions; this can be done by making periodic sweeps of the panels characteristics and has according to [3] already been implemented by others.

Considering the narrow distributions of the MPP of the unshadowed panels in Fig. 4.1 an alternative approach would be to view the V_{MPP} as fixed instead of using a true MPPT, but judging from the wide distribution of the shadowed panels and the power loss curve shown in Fig. 4.2 this method would give severe power-loss when shaded. According to Amparo Solutions AB, shading during operation cannot be ruled out and using a fixed V_{MPP} is therefore not recommended.

From the results in section 4.1.2 it is clear that it is more important to operate in close vicinity to the V_{MPP} than to minimize the ripple, since the momentaneous power loss is much greater than the average power loss by symmetric deviation from V_{MPP} .

It has also been shown that controlling several solar panels at their individual MPPT would be possible using only one DC-DC converter. Several pitfalls have been addressed in section 3.3.3, but trials on a real hardware platform is recommended to further investigate possible problems with this novel approach.

5.1 Future work

Although this study concludes the feasibility of incremental conductance for this specific hardware setup, the results concerning efficiency presented in section 4.2.2 will in reality be less, considering miscellaneous losses in the electronics. It would therefore be recommended to include models to account for the losses and then perform further optimization of the efficiency than just of the step size; for example capacitance size and sampling frequency. Even though stability has been shown in cases of high and low solar insolation, this should of course be reevaluated when introducing the losses.

References

- [1] Soumitro Banerjee and George C. Verghese. *Nonlinear Phenomena in Power Electronics - Attractors, Bifurcations, Chaos, and Nonlinear Control*, pages 1–6. John Wiley & Sons, 2002.
- [2] S.L. Brunton, C.W. Rowley, S.R. Kulkarni, and C. Clarkson. Maximum power point tracking for photovoltaic optimization using ripple-based extremum seeking control. 2009.
- [3] T. Eswam and P.L. Chapman. Comparison of photovoltaic array maximum power point tracking techniques. *IEEE Transactions on Energy Conversion*, 22(2):439–449, 2007.
- [4] SCHOTT Solar GmbH. ASI[®] OEM outdoor solar modules. (Electronic), 2007. Available: http://www.schottsolar.com/fileadmin/media/sales-services/downloads/product-information/oem-solar-modules/ASI_OEM_Outdoor.pdf (2009-06-23).
- [5] SCHOTT Solar GmbH. ASI[®]-OEM-solarmodules for outdoor, available standard module designs. (Electronic), 2007. Available: http://www.schottsolar.com/fileadmin/media/sales-services/downloads/product-information/oem-solar-modules/TM_55_010_ASI_OEM_Outdoor_available_designs.pdf (2009-06-23).
- [6] W. Herrmann, W. Wiesner, W. Vaassen, U. GmbH, and G. Cologne. Hot spot investigations on PV modules-new concepts for a test standard and consequences for module design with respect to bypass diodes. In *IEEE Photovoltaics Specialists Conference*, volume 26, pages 1129–1132. IEEE Inc, 1997.
- [7] DP Hohm and ME Ropp. Comparative study of maximum power point tracking algorithms. *Progress in Photovoltaics*, 11(1):47–62, 2003.
- [8] P. Horowitz and W. Hill. *The art of electronics*. University Press, 1989.
- [9] KH Hussein, I. Muta, T. Hoshino, and M. Osakada. Maximum photovoltaic power tracking: an algorithm for rapidly changing atmospheric conditions. *IEE Proceedings-Generation Transmission and Distribution*, 142(1):59–64, 1995.
- [10] J.W. Kimball and P.T. Krein. Digital ripple correlation control for photovoltaic applications. *Urbana*, 51:61801.
- [11] Antonio Luque and Steven Hegedus, editors. *Handbook of Photovoltaic Science and Engineering*. John Wiley & Sons, 2003.
- [12] P.J. Mohr, B.N. Taylor, and D.B. Newell. CODATA Recommended Values of the Fundamental Physical Constants: 2006.
- [13] A. Ortiz-Conde, F.J. García Sánchez, and J. Muci. New method to extract the model parameters of solar cells from the explicit analytic solutions of their illuminated I–V characteristics. *Solar Energy Materials and Solar Cells*, 90(3):352–361, 2006.
- [14] F.C Treble. Solar cells. volume 127, pages 505–527, 1980.
- [15] H.L. Tsai, C.S. Tu, and Y.J. Su. Development of Generalized Photovoltaic Model Using MATLAB/SIMULINK. 2008.
- [16] A. Woyte, J. Nijs, and R. Belmans. Partial shadowing of photovoltaic arrays with different system configurations: literature review and field test results. *Solar Energy*, 74(3):217–233, 2003.

A Solar panels

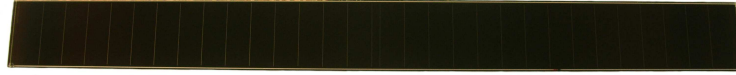


Figure A.1: Solar panel, SCHOTT 1073494

Fig. A.1 shows the solar panels used in this thesis: ASI 3 Oo 15x2/576/054 FA, manufactured by SCHOTT Solar AG, partnumber 1073494. Each panel consists of 30 cells divided into two parts, so each panel is actually two. The data in table A.1 is for a whole panel of 30 cells [5].

Open-circuit voltage	24.5 V
Voltage at nominal power	18 V
Short-circuit current	120.3 mA
Current at nominal power	91.2 mA
Nominal power	1641 mW
<hr/>	
Length	576 mm
Width	54 mm
Thickness	3.2 mm

Table A.1: Solar panel data at an illumination of $100mW/cm^2$

B Measurement circuit

The main part of the circuit is shown in Fig. B.1, where the 8 solar panels are connected by setting the respective digital input, $SP1-SP8$, high and the load on the connected panel is controlled by the analog input $Aout$. The operational amplifier and its surrounding components, form an electronic load. A simple voltage divider (R1-R2) is used to be able to measure up to 30V with the DAQ device that only supports voltages up to 10V.

The part of the circuit used for measuring light and temperature is shown in Fig. B.2. Since the solar panels are double and actually contain two panels, the amount is stated as 4 but with 8 designators.

Type	Name/Value	Quantity	Designator
Capacitor	50nF	1	C1
Capacitor	1 μ F	3	C2-C4
Capacitor	100nF	2	C5-C6
Diode	Zener 15V	9	D1-D9
Light Sensor	SFH 5711-2/3-Z	3	IC2-IC4
MOSFET	STP36NF06FP	1	Q1
MOSFET	PHP21N06LT	8	Q2-Q9
Operational Amplifier	MC33201PG	1	IC1
Relay	G6K-2F-Y 5VDC	8	K1-K8
Resistor	470k Ω 0.25W	1	R1
Resistor	220k Ω 0.25W	1	R2
Resistor	8.2k Ω 0.25W	1	R3
Resistor	1.8k Ω 0.25W	1	R4
Resistor	18 Ω 0.25W	1	R5
Resistor	10k Ω 0.25W	6	R6,R14-R18
Resistor	1k Ω 0.25W	1	R7
Resistor	3.3k Ω 0.25W	8	R8-R13,R19-R20
Solar Panel	ASI 3 Oo 15x2/576/054 FA	4	SP1-SP8
Thermistor	2381 640 55103	2	R21-R22

Table B.1: Bill of materials

All resistors were measured prior to soldering, so that a higher precision of circuit calculations were possible. The measurements were done using an Agilent 34410A digital multimeter, with the results presented in table B.2.

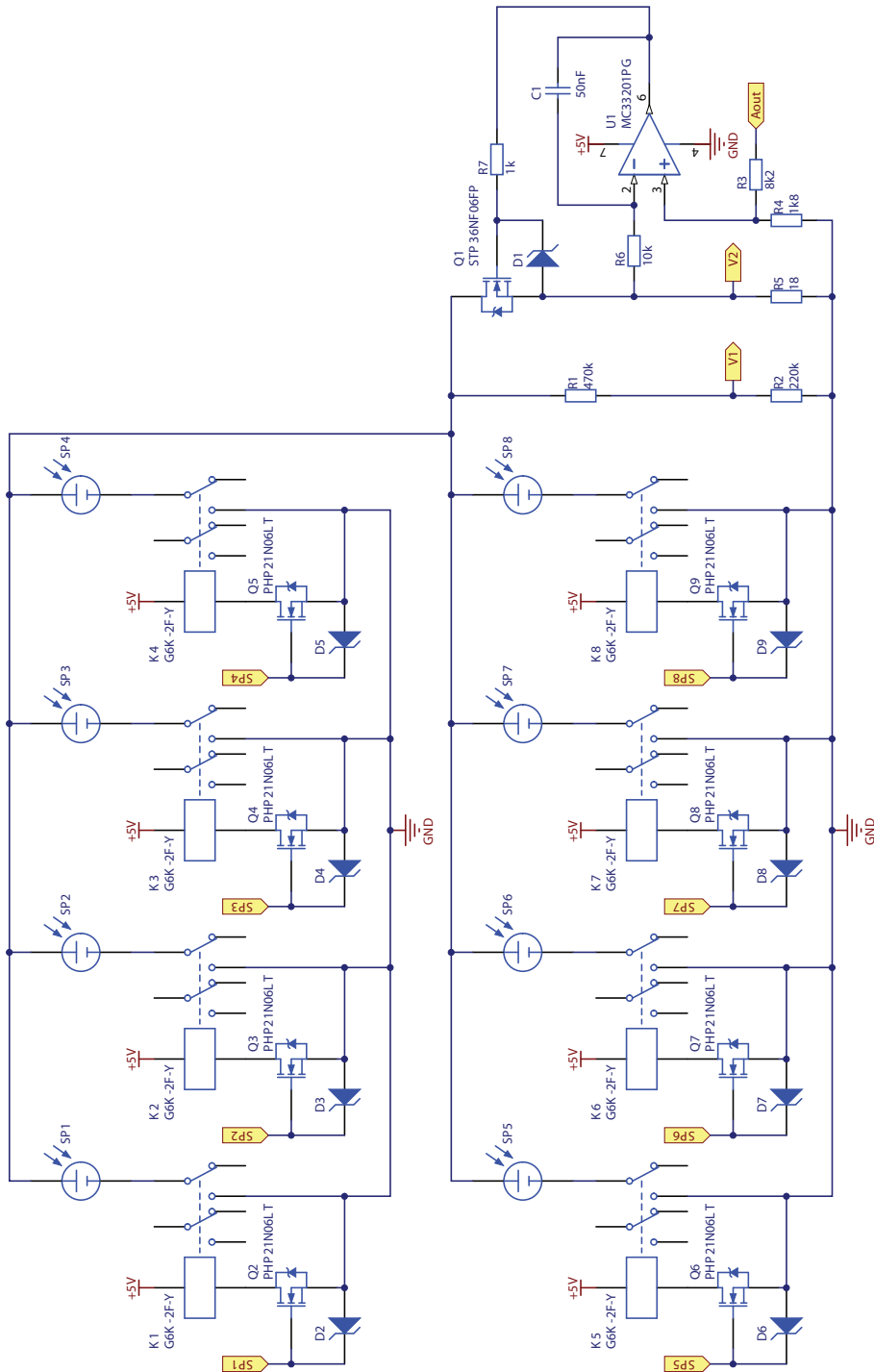


Figure B.1: Measurement circuit for current and voltage

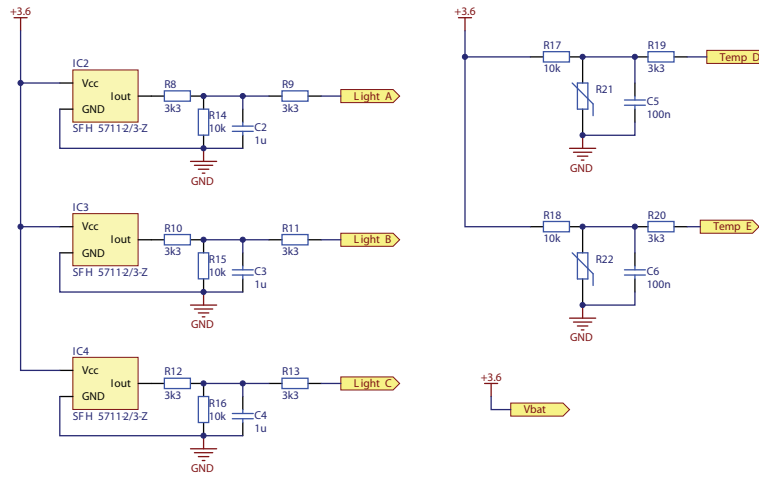


Figure B.2: Measurement circuit for light and temperature

Designator	Value
R1	469.83k Ω
R2	221.55k Ω
R3	8.2076k Ω
R4	1.7807k Ω
R5	17.960 Ω
R6	10.054k Ω
R7	0.99499k Ω
R8	3.2858k Ω
R9	3.2609k Ω
R10	3.2680k Ω
R11	3.2534k Ω
R12	3.3105k Ω
R13	3.3263k Ω
R14	10.043k Ω
R15	10.089k Ω
R16	10.066k Ω
R17	10.061k Ω
R18	10.076k Ω
R19	3.2663k Ω
R20	3.2694k Ω

Table B.2: Measured resistance values